Annals of Botany **129**: 303–313, 2022
https://doi.org/10.1093/aob/mcab143, available online at www.academic.oup.com/aob

ANNALS OF BOTANY
Founded 1887

Phylogenetic, ecological and intraindividual variability patterns in grass phytolith shape

Kristýna Hošková[1,2,*], Jiří Neustupa[1], Petr Pokorný[3] and Adéla Pokorná[1,4]

[1]Department of Botany, Faculty of Sciences, Charles University in Prague, Benátská, 2, CZ-128 01 Praha 2, Czech Republic, [2]Institute of Botany, Academy of Science of the Czech Republic, CZ-252 43 Průhonice, Czech Republic, [3]Center for Theoretical Study, Joint Research Institute of Charles University and Czech Academy of Sciences, Husova 4, CZ-110 00 Praha 1, Czech Republic and [4]Institute of Archaeology, Czech Academy of Sciences, Letenská 4, CZ-11801 Praha 1, Czech Republic
** For correspondence. E-mail kristyna.kuncova@natur.cuni.cz*

Received: 13 August 2021 Returned for revision: 16 November 2021 Editorial decision: 22 November 2021 Accepted: 26 November 2021
Electronically published: 29 November 2021

• **Background and Aims** Grass silica short cell (GSSC) phytoliths appear to be the most reliable source of fossil evidence for tracking the evolutionary history and paleoecology of grasses. In recent years, modern techniques that quantitatively assess phytolith shape variation have widened opportunities for the classification of grass fossil phytoliths. However, phylogenetic, ecological and intraindividual variability patterns in phytolith shape remain largely unexplored.
• **Methods** The full range of intraindividual phytolith shape variation [3650 two-dimensional (2-D) outlines] from 73 extant grass species, 48 genera, 18 tribes and eight subfamilies (particularly Pooideae) was analysed using geometric morphometric analysis based on semi-landmarks spanning phytolith outlines.
• **Key Results** The 2-D phytolith shape is mainly driven by deep-time diversification of grass subfamilies. There is distinct phytolith shape variation in early-diverging lineages of Pooideae (Meliceae, Stipeae). The amount of intraindividual variation in phytolith shape varies among species, resulting in a remarkable pattern across grass phylogeny.
• **Conclusions** The phylogenetic pattern in phytolith shape was successfully revealed by applying geometric morphometrics to 2-D phytolith shape outlines, strengthening the potential of phytoliths to track the evolutionary history and paleoecology of grasses. Geometric morphometrics of 2-D phytolith shape is an excellent tool for analysis requiring large numbers of phytolith outlines, making it useful for quantitative palaeoecological reconstruction.

Key words: Paleoecology, grass phylogeny, phytoliths, geometric morphometrics, semi-landmarks, Pooideae.

INTRODUCTION

Phytoliths are microscopic particles of silica formed in certain plants that have great potential to track the evolutionary history and paleoecology of grasses (Poaceae) (Strömberg, 2005, 2011, 2015; Prasad *et al.*, 2011). Composed largely of biogenic opaline silica ($SiO_2 \cdot nH_2O$), phytoliths are preserved in various sedimentary environments, even when other grass fossils are not (Piperno, 2006; Strömberg *et al.*, 2018). Grass phytoliths, and particularly grass silica short cell (GSSC) phytoliths, are known to vary in shape at multiple taxonomic levels (subfamilies, tribes and sometimes even genera; Metcalfe, 1960; Mulholland and Rapp, 1992; Piperno and Pearsall, 1998; Rudall *et al.*, 2014), whereas other grass fossil remains such as pollen, leaves or seeds are either rare or not taxonomically informative below the family level (Jacobs *et al.*, 1999; but for the case of pollen, see Mander *et al.*, 2013). Gallaher *et al.* (2020), investigating 70 species of early-diverging grasses, plus Oryzoideae and Bambusoideae, quantitatively documented that GSSC phytolith 3-D shape carries a strong phylogenetic signal, that can distinguish grass subfamilies and tribes. However, phylogenetic, ecological and intraindividual variability patterns in phytolith shape in other grass taxonomic groups remain unexplored.

Most of grass diversity is found in two clades: the BOP (Bambusoideae, Oryzoideae and Pooideae) and PACMAD (Panicoideae, Arundinoideae, Chloridoideae, Micrairoideae, Aristidoideae and Danthonioideae) (Strömberg, 2011; Soreng *et al.*, 2015, 2017). Twiss *et al.* (1969) proposed three major divisions of GSSC phytoliths corresponding to the three dominant grass subfamilies native to the Great Plains of the USA: bi-/poly-lobate/cross in Panicoideae; saddle in Chloridoideae; and circular/oblong/rectangular in Pooideae. These divisions are mainly useful in regions where grasses are abundant and diverse at the subfamily taxonomic level [e.g. in grasslands of the North American Great Plains (Fredlund and Tiezsen, 1994) and sub-Saharan Africa (Bremond *et al.*, 2005; Barboni *et al.*, 2007)]. However, they are less informative in regions where only one subfamily has dominated long term, such as large areas of temperate and boreal regions of Eurasia, where subfamily Pooideae prevails (Gibson, 2009).

Pooideae is the largest Poaceae subfamily, with almost 4000 species, most of them adapted to open areas experiencing frost (Bouchenak-Khelladdi *et al.*, 2010; Edwards and Smith, 2010; Soreng *et al.*, 2017; Schubert *et al.*, 2019*a*, *b*). While considerable effort has been made to refine the categorization

of phytolith shape variation within subfamilies Panicoideae, Chloridoideae, Bambusoideae and Oryzoideae (Lu and Liu 2003; Fahmy, 2008; Novello *et al.*, 2012; Cai and Ge, 2017; Neumann *et al.*, 2017; Gallaher *et al.*, 2020), phytolith shape variation in Pooideae is largely unexplored, with only a handful of studies touching on this area, such as investigations of Stipa-type phytoliths (Mullholand, 1989; Gallego and Distel, 2004; Silantyeva *et al.*, 2018).

Individual grass subfamilies are mostly adapted to certain environmental conditions and tend to prevail in specific vegetation zones (Gibson, 2009). In phytolith analysis, this association is used to define indices that can be applied as proxies of past environments. For example, the aridity index (Iph; Diester-Haass *et al.*, 1973; Alexandre *et al.*, 1997), calculated as the proportion of Chloridoideae, commonly found in arid conditions and producing saddle-shaped morphotypes, and Panicoideae, commonly found in more humid conditions and producing bilobates and crosses, is used as a proxy for aridity in past ecosystems. Similarly, the climatic index (Ic; Twiss, 1992) reconstructs past climates on the basis of the proportion of morphotypes characteristic of Pooideae, adapted to open and cold environments (rondels), vs. the amount of morphotypes characteristic of Chloridoideae and Panicoideae, which are adapted to higher temperatures. However, it is untenable to use phytolith spectra *per se* for the indication of past habitat conditions without a knowledge of the distribution of phytolith variation across the phylogenetic tree, including the proportion of intraspecific variation.

Our recent study (Hošková *et al.*, 2021) observed very low GSSC phytolith shape plasticity between populations of the same species compared with interspecific variation, in a hierarchically designed study of two grass species with restricted ecological niches (*Brachypodium pinnatum* and *B. sylvaticum*), which allowed us to assume minor phytolith shape variation due to environmental conditions. However, significant residual variation (51 % of the total variation, which was not captured by the defined levels: species, populations, individuals, leaves and parts of leaves) was related to the intraindividual variation of phytolith shape within the individual sample. This type of variation (which is intrinsic to phytoliths and not present in other microfossils) results from the fact that each grass species produces more than one phytolith morphotype, resulting in an overlap of phytolith shapes between taxa (e.g. Rovner and Russ, 1992). Whether the phytolith is formed over the veins (costal) or between the veins (intercostal) has also been reported as another source of intraindividual phytolith shape variation (Metcalfe, 1960; Gallaher *et al.*, 2020). Piperno and Pearsall (1998), in their seminal work, proposed that intraindividual variation in phytolith shape may be lineage specific; species could vary in the amount of intraindividual phytolith shape variation based on their position in the phylogenetic tree. Knowledge of the full range of intraindividual variation could improve our understanding of the phylogenetic pattern in phytolith shape.

To quantify the proportion of intraindividual variation in relation to the phylogenetic pattern in phytolith shape, we used methods of geometric morphometrics (Hošková *et al.*, 2021). We explored whether GSSC phytolith shapes changed in response to diversification during grass evolution and how closely phytolith shapes reflect phylogenetic relationships in the Poaceae family. Because the degree of intraindividual variation in phytolith shape in most grasses has never been explored, we aimed to separate intraindividual variation from phylogenetic variation. We particularly focused on grass subfamily Pooideae, adapted to open areas experiencing frost, examining the potential affinity of ecological adaptation of species for phytolith shape variation within this taxon.

Geometric morphometrics is one of the most frequently applied techniques in biological shape analysis today (Polly and Motz, 2016), enabling size to be effectively removed and focusing purely on the analysis of shape, allowing the simple collection of co-ordinate data and easy visualization of results as transformations of shapes themselves rather than as tables of numbers (Bookstein, 1989; Klingenberg, 2013). Unlike the traditional description of pre-defined phytolith morphotypes {International Code for Phytolith Nomenclature 2.0 [International Committee for Phytolith Taxonomy (ICPT), 2019]}, geometric morphometrics allow quantification and visualization of continuous phytolith shape variation. Different phytolith morphotypes are analysed together within a single multivariate space (morphospace), allowing exploration of major trends in shape variation. It should be noted that similar analyses aimed at representing phytolith variability have in the past been based on morphometric analyses yielding the univariate shape parameters of individual objects (Russ and Rovner, 1989; Ball *et al.*, 2016; Yost *et al.*, 2021). In addition, techniques closely related to geometric morphometrics are based on the representation of the phytolith shape features by the elliptic Fourier analysis, which yields a series of elliptic Fourier descriptors while retaining the outline shape features of analysed objects (Evett and Cuthrell, 2016; Cai and Ge, 2017). The Procrustes superimposition method, the core of geometric morphometric analysis, relies on the point-to-point correspondence of individual landmarks among the analysed specimens. In 2-D phytolith outlines, these points are represented by a series of equidistant semi-landmarks. For phytoliths having symmetric 2-D shapes, there may be two or more fixed points delimiting individual symmetric curves. These points are typically derived from the orientation of phytoliths within plant tissue (Hošková *et al.*, 2021).

MATERIALS AND METHODS

Plant material processing

A total of 3650 modern grass phytoliths from 73 species, 48 genera, 18 tribes and eight subfamilies were analysed (see Supplementary data Table S1).

Plant material was processed following the *in situ* charring method of Kumar *et al.* (2017). This method preserves the original phytolith position within the plant epidermis. One leaf per plant per species was sampled. Leaves were cleaned in an ultrasonic cleaner (Digital Ultrasonic Cleaner CE-7200A). A segment of leaf was laid on a glass slide. Small pieces of folded aluminium foil were placed near the two shorter sides of the slide. Another glass slide was placed on top of the slide, holding the sample in place. The aluminium foil between the slides prevents them from sticking together. Slides were put into a muffle furnace at 550 °C for 5 h. The slides containing burnt material were washed with 1 N HCl and distilled water (using a pipette).

After the slides dried, plant material remaining on the bottom slide was covered with one drop of 15 % glycerol solution and a cover slide. Slides were then analysed using transmission light microscopy (Leica DM 1000 LED).

Data acquisition

Sequential microphotographs of rows of GSSC phytoliths in the charred epidermis were acquired under ×400 magnification (Leica camera ICC50 W). The planar view of GSSC costal (over veins) phytolith morphotypes with a long axis parallel with the long axis of the leaf was chosen for analysis. First, two fixed landmarks were placed at the phytolith edges perpendicular to the longest axis of the leaf (Fig. 1; Supplementary data Fig. S1). Then, 48 equidistant points were placed along both outline halves, resulting in 96 points treated as semi-landmarks in the subsequent geometric morphometric analysis. For each individual phytolith image (3650 in total), 98 two-dimensional

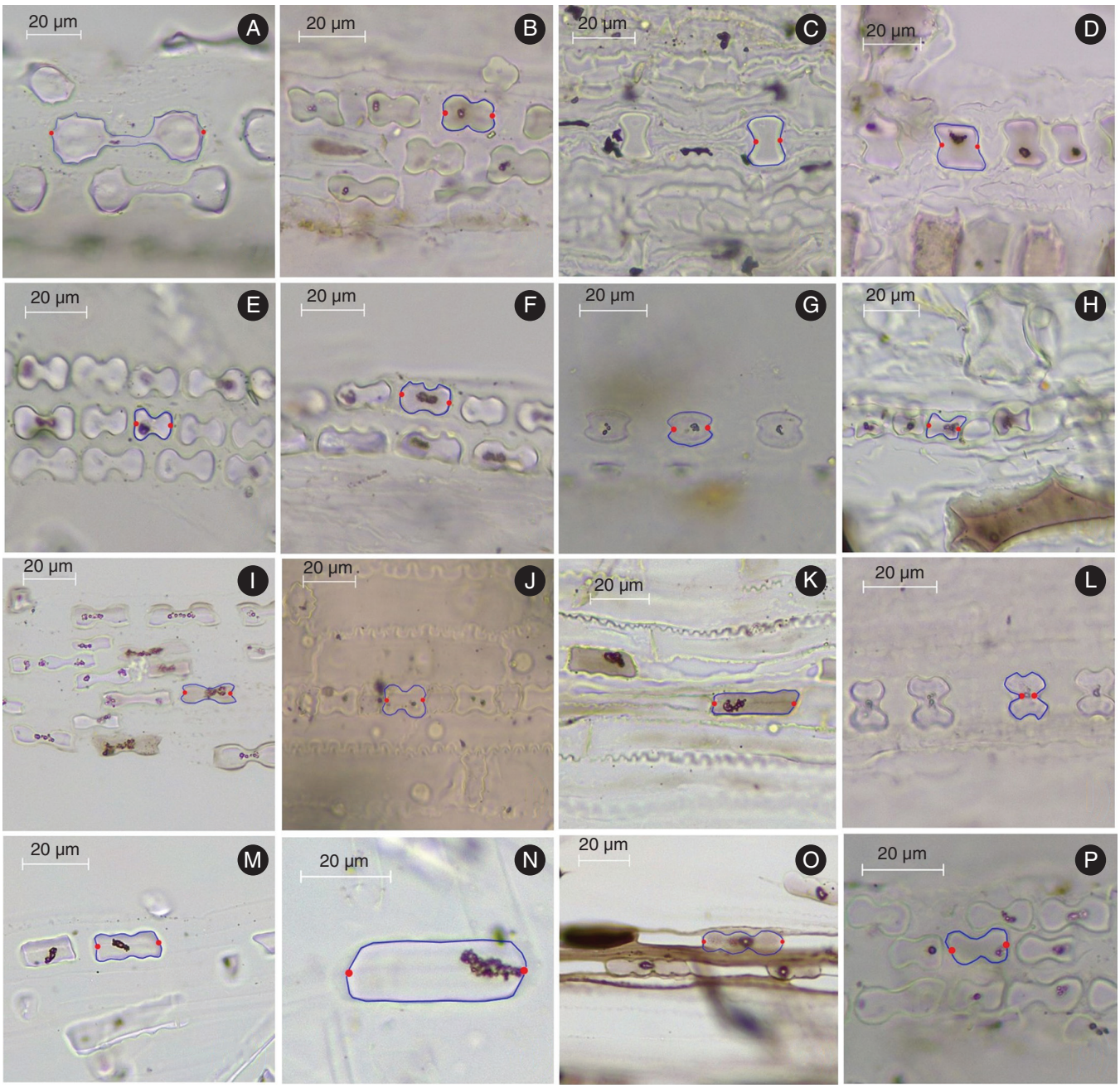

FIG. 1. Microphotographs of charred grass epidermises with GSSC phytoliths. Red dots indicate two fixed landmarks; blue lines indicate the phytolith outline with 96 equidistant semi-landmarks. (A) *Aristida rhiniochloa*, Aristidoideae; (B) *Hakonechloa macra*, Arundinoideae; (C) *Bambusa tuldoides*, Baumbusoideae; (D) *Arundinaria gigantea*, Bambusoideae; (E) *Danthonia alpina*, Danthonioideae; (F) *Schismus arabicus*, Danthonioideae; (G) *Cynodon dactylon*; (H) *Brachyelytrum erectum*, Pooideae; (I) *Bothriochloa ischaemum*, Panicoideae; (J) *Coix lacryma-jobi*, Panicoideae; (K) *Alopecurus pratensis*, Pooideae; (L) *Zizania latifolia*, Oryzoideae; (M) *Bromus erectus*, Pooideae; (N) *Holcus lanatus*, Pooideae; (O) *Melica picta*, Pooideae; (P) *Stipa sibirica*, Pooideae.

points were digitized. This approach was only applied to phytolith morphotypes bilobate, polylobate, saddle, crenate and trapezoid observed in planar view {International Code for Phytolith Nomenclature 2.0 [International Committee for Phytolith Taxonomy (ICPT), 2019]}; rondels, positioned in the leaf epidermis in planar view, had no identifiable landmarks and were not analysed. During plant material processing, segments of leaves were laid on a glass slide with random orientation regarding abaxial–adaxial leaf sides. The outer periclinal surface of phytoliths was chosen for phytolith outline analysis because this surface has edges that are clear, distinct and well defined under light microscopy. Digitization utilized the semi-automated background curves tool in freely available TpsDig, ver. 2.31 (Rohlf, 2015). Equidistant positions of semi-landmarks along the outlines relative to the positions of the fixed landmarks were obtained using the 'digit.curves' function in GEOMORPH v. 3.3.2 (Dryden and Mardia, 2016; Adams *et al.*, 2021), in R v. 3.6.3 (R Core Team, 2020) (for a summarized methodological workflow see Supplementary data Table S2).

Data analysis

Generalized Procrustes analysis of phytoliths with biradial symmetry. Geometric morphometrics was performed on a dataset of 3650 phytolith configurations, each consisting of 98 landmark co-ordinates (following Hošková *et al.*, 2021). The 2-D shape of phytoliths in planar view (the long axis of the phytolith parallel with the long axis of the leaf) exhibits symmetry, meaning that left–right and upper–lower parts of the 2-D outline are not differentiated. To achieve correspondence of all phytolith configurations, we applied geometric morphometrics for the analyses of biradial symmetry (Savriama *et al.*, 2010, 2012; Savriama and Klingenberg, 2011; Neustupa, 2013) (see also Supplementary data Fig. S1). A generalized Procrustes analysis, which minimizes the sum of squared distances between corresponding landmarks to extract shape data by removing the extraneous information of size, location and orientation, was applied (e.g. Zelditch *et al.*, 2012; Dryden and Mardia, 2016). The semi-landmark position was optimized by iterative sliding along the curve tangents to achieve the lowest bending energy yielding the smoothest possible deformation between each configuration and the mean shape (Bookstein, 1997; Pérez *et al.*, 2006; Gunz and Mitteroecker, 2013). Original phytolith configurations were transformed and re-labelled, and then subjected to generalized Procrustes analysis. The resulting multiplied dataset consisted of Procrustes co-ordinates of original configurations and transformed and re-labelled copies (a reflected copy about the horizontal adaxial–abaxial axis; a reflected copy about the vertical left–right axis; and a reflected copy about both axes) (Savriama and Klingenberg, 2011; Klingenberg, 2015; Savriama, 2018; Hošková *et al.*, 2021). By averaging the original configuration and transformed copies of each specimen, symmetrized phytolith configurations that are symmetric and invariant under all transformations were obtained. Generalized Procrustes analysis was conducted using the 'procGPA' function in SHAPES v. 1.2.5 in R v. 3.6.3.

Quantification of symmetric and asymmetric components of shape variation. Principal component analysis (PCA) was conducted with the superimposed Procrustes co-ordinates consisting of all the original configurations and their transformed copies. This PCA separated components of symmetric shape variation (variation between symmetrized configurations) from three components of asymmetry (asymmetry under reflection in the adaxial–abaxial direction, asymmetry in the left–right direction and asymmetry regarding both these axes) (Savriama *et al.*, 2010; Klingenberg, 2015). Proportions of variation in the sub-spaces of biradial symmetry and three asymmetric patterns were quantified by summing percentages of variance explained by PCs belonging to a given sub-space using scores from principal components (PCs) obtained by 'procGPA' function in SHAPES v. 1.2.5 in R v. 3.6.3.

Quantification of different sources of shape variation. Different sources of shape variation among phytoliths were quantified by multivariate Procrustes analysis of variance (ANOVA) of the symmetrized configurations of individual phytoliths (e.g. Klingenberg, 2015). Data were analysed in a nested structure reflected by the Procrustes ANOVA models, decomposing the matrix of Procrustes distances among individual configurations into different sources specified by the independent factors. Besides quantifying the Procrustes sum of squares (SS) spanned by each factor and its proportion of the total variation (η^2), the significance of the effects was evaluated by comparing their original Procrustes SS values with their random distribution yielded by 999 permutations (Schaefer *et al.*, 2006; Neustupa and Woodard, 2021). The randomization design reflected the nested structure of the independent factors. The main effect, evaluating the differentiation of phytoliths of the BOP and PACMAD lineages, was tested against the random distribution based on repeated reshuffling of individual subfamilies between BOP and PACMAD. Likewise, the SS spanned by the 'subfamily' effect nested within 'BOP vs. PACMAD' was evaluated by comparison with the random distribution yielded by reshuffling tribes among subfamilies within the BOP and PACMAD groups. The effect of tribes was tested against the random SS distribution by reshuffling species among tribes. Differentiation of phytoliths by species was evaluated by randomization of individual specimens. (The effect of genera was not tested due to the low number of observations per genus in most cases.) The function 'procD.lm' in GEOMORPH v. 3.3.2 (Dryden and Mardia, 2016; Adams *et al.*, 2021), in R v. 3.6.3 (R Core Team, 2020) was used to decompose sources of phytolith shape variation. Pairwise randomized residual permutation procedure post-hoc tests were performed using 'pairwise' function in RRPP v. 0.5.2 in R v. 3.6.3.

Amount of intraindividual variation in phytolith shape in individual grass species. The amount of intraindividual phytolith shape variation in individual grass species, represented by average Procrustes distances of individual phytoliths to species centroids, was compared using the function 'betadisper' in VEGAN (Oksanen *et al.*, 2019) in R v. 3.6.3.

Phylogenetic signal in grass phytolith shape and classification of phytoliths. Grass phylogeny was generated using the S3 scenario with function 'phylo.maker' in V.PHYLOMAKER v.0.1.0 in R v. 3.6.3 (Jin and Qian, 2019) using a 'backbone' tree based on molecular data from seed plant phylogeny (mega-tree

'GBOTB.extended.tre'; Smith and Brown, 2018). Out of the 73 species examined, 54 were in the Smith and Brown (2018) backbone tree, with the rest added using the S3 scenario of Jin and Qian (2019).

To visualize the phylogenetic history of phytolith shape change, grass species positions along PC1, as well as PCs representing different components of asymmetric variation, were mapped on the grass phylogeny tree. Intraindividual shape variation, measured by averaged distances from the species group centroid in multivariate space, was also mapped on the grass phylogeny. We used function 'phylosig' in R/PHYTOOLS v. 0.7.47 (Revell, 2012) to determine Pagel's lambda, a measure of phylogenetic signal in individual components of the shape data (individual PCA axes, amount of intraindividual variation); function 'pgls' in R/CAPER v. 1.0.1 to calculate confidence intervals (Orme *et al.*, 2018); and function 'contMap' to visualize the phylogenetic history of individual components of the shape data, using the function 'fastAnc' in R/PHYTOOLS v. 0.7.47 to reconstruct maximum likelihood values at tree nodes (Revell, 2012).

To test whether individual phytoliths can be assigned to predefined subfamilies and tribes based on phytolith shape, linear discriminant analysis (LDA) was conducted. From multiple measures on different specimens, LDA seeks a linear combination (the discriminant function) that maximizes the ratio of the between-group SS to the within-group SS (e.g. Mitteroecker and Bookstein, 2011). A specimen with unknown group affiliation can be assigned to one of the groups based on its score for this linear combination. Here, variables (Procrustes co-ordinates) were reduced by PCA on symmetrized phytolith shape variation prior to LDA. Thus, LDA was based on the first 27 PCs (each component explaining >0.001 % of total variation). The analysis yielded the discriminant function which, applied to the dataset again, resulted in the proportion of correctly classified individual phytoliths. LDA was conducted in PAST ver. 4.05 (Hammer *et al.*, 2001).

To visualize the discrimination of grass subfamilies by their phytolith shape, canonical variates analysis (CVA) was performed on symmetrized phytolith shape configurations in MorphoJ (Klingenberg, 2011).

RESULTS

Decomposition of symmetric and asymmetric variation in phytolith shape

The first group of PCs, associated with entirely symmetric shape variation highlighting the differences among individual phytoliths, accounted for 89.5 % of the total shape variation of the dataset. The second group of PCs, associated with three sub-spaces of asymmetric shape variation illustrating the effects of shape asymmetry among individual parts of each phytolith, accounted for 11.0 % of the total variation. The PCA results indicated that phytolith shape variation consists mainly of shape differences among individual phytoliths and relatively little shape asymmetry within phytoliths (e.g. between their left and right sides). Therefore, in the following analyses of phytolith shape, we considered only the dataset of the symmetrized phytolith configurations.

Sources of variation in phytolith shape

Individual taxonomic levels accounted for 81.9 % of the total variation in symmetric phytolith shapes (Table 1). Residual variation consisting of phytolith shape variation, within individuals, was considerably lower (18.2 %). Variation between subfamilies contributed the most (42.7 %, $P = 0.001$), followed by variation between species (23.8 %, $P = 0.001$) and tribes (14.0 %, $P = 0.001$). Phytolith shape variation between PACMAD and BOP clades accounted for only 1.4 % of the total variation ($P = 0.7$).

Significant differences in phytolith shape were found for all 28 subfamily pairs in the post-hoc pairwise tests (at the significance level of 0.01) (Supplementary data Table S3).

Intraindividual phytolith shape variation across species

The amount of intraindividual GSSC phytolith shape variation differed across species (Fig. 2; see also Supplementary data Table S4). We reported variation from bilobate to saddle-shaped phytoliths in *Eragrostis minor* and from bilobate to polylobate-shaped phytoliths in *Brachypodium dystachion*, *B. pinnatum*, *Bromus inermis*, *Calamagrostis epigejos*, *Bothriochloa ischaemum*, *Coix lacryma-jobi* and *Digitaria sanguinalis*. However, it should be noted that resemblance to traditionally defined morphotypes (bilobates, saddles) may be due to the 2-D nature of this study and could be reconsidered by observing 3-D characteristics. Other species, such as *Bromus erectus* (tribe Bromeae), *Melica picta* (tribe Meliceae), *Festuca gigantea*, *Festuca arundinacea*, *Helictotrichon pubescens*, *Milium effusum*, *Phleum pratense, Poa nemoralis* and *Trisetum flavescens* (tribe Poeae) significantly varied intraindividually in the length and width of GSSC phytoliths (the so-called crenate morphotype). *Ehrharta erecta* (tribe Ehrharteae) varied intraindividually in the length of the polylobate phytolith shape, whereas *Brachyelytrum erectum* (tribe Brachyelytreae), *Dichanthium annulatum* (tribe Andropogoneae) and *Echinochloa crus-galli* (tribe Paniceae) varied intraindividually in the length of the bilobate shape. In contrast, some species were very conservative in their phytolith shape, including *Bambusa tuldoides*, *Phragmites australis* and *Aristida rhinochloa*.

Mapping phytolith shape data onto the phylogeny

According to the PCA performed on symmetrized phytolith configurations, the first two PCs explained >96 % of the total

Table 1. *Results of the Procrustes ANOVA evaluating different sources of variation in symmetrized phytolith shape*

Source	d.f.	SS	MS	η^2	P
BOP × PACMAD	1	0.742	0.742	0.014	0.7
Subfamily (BOP × PACMAD)	6	22.861	3.81	0.427	0.001***
Tribe (subfamily)	10	7.465	0.747	0.140	0.001***
Species (tribe)	56	12.725	0.227	0.238	0.001***
Residuals	3576	9.713	0.003	0.182	
Total	3649	53.506			

d.f., degrees of freedom; SS, sum of squares; MS, means squares; η^2, proportion on the total variation; P, probability of the null hypothesis. ***$P < 0.001$.

variation (Fig. 3). Along PC1 (explaining 89.5 % of the total variation), phytoliths varied from elongated shapes with two deeply incised lobes to shorter and taller shapes on opposite sides. Along PC2 (explaining 7.0 % of the total variation), phytolith shape varied from shorter outlines with two deeply incised lobes to elongated shapes with a pronounced middle part on the opposite sides.

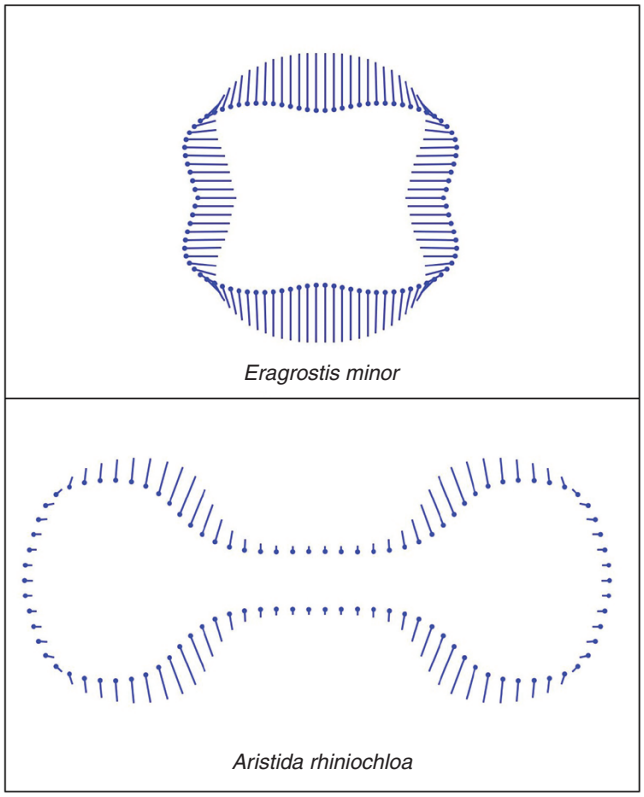

FIG. 2. The amount of intraindividual variation in phytolith shape (represented by the average distance of individual phytolith to species centroid) is visualized by 'lollipop' graphs where the stick of the lollipop indicates the direction of the variation, whereas the lollipops (filled dots) together represent the mean phytolith shape outline. *Aristida rhinochloa* represents species with less variable phytolith shape, whereas *Eragrostis minor* has a highly variable phytolith shape. (For phytolith outlines of more species, see also Supplementary data Table S4.).

To visualize the phylogenetic history of symmetric phytolith shape change, we mapped PC1 scores of each grass species on the grass phylogeny tree (Fig. 4). The most prominent shape variation in the data – an elongated shape with two deeply incised lobes vs. shorter and taller shapes – was strongly phylogenetically conserved at the subfamily level: phytolith shapes of individual monophyletic subfamilies were substantially different. However, similar phytolith shapes occurred in each of two major grass subclades: BOP and PACMAD. The measure of phylogenetic conservatism (Pagel's lambda) for individual PCs describing symmetrized shape variation, along with the measure of phylogenetic conservatism in asymmetric components of shape variation and in the amount of intraindividual variation (Supplementary data Fig. S2) are summarized in Table 2. Pagel's lambda is a multiplication constant used to transform a phylogenetic tree; in a lambda-transformed tree, the internal branch lengths of the phylogeny are multiplied by it. Lambda = 1 hence indicates a full phylogenetic signal corresponding to Brownian motion evolution and lambda = 0 indicates complete phylogenetic randomness (all internal lengths are set to zero, resulting into a star-like phylogeny). Lambda value for the given set is estimated by maximum likelihood.

The phylogenetic signal in the shape data was apparent from the distinctive position of individual grass subfamilies in the morphospace of phytoliths averaged by species (Fig. 5). Linear discriminant analysis of overall (including intraindividual) phytolith shape variation classified by subfamilies (Supplementary data Table S5) and by tribes in Pooideae (Supplementary data Table S6) showed high rates of correct classifications (>70 %) in subfamilies Pooideae, Aristidoideae, Bambusoideae and Oryzoideae, and tribes Meliceae and Stipeae.

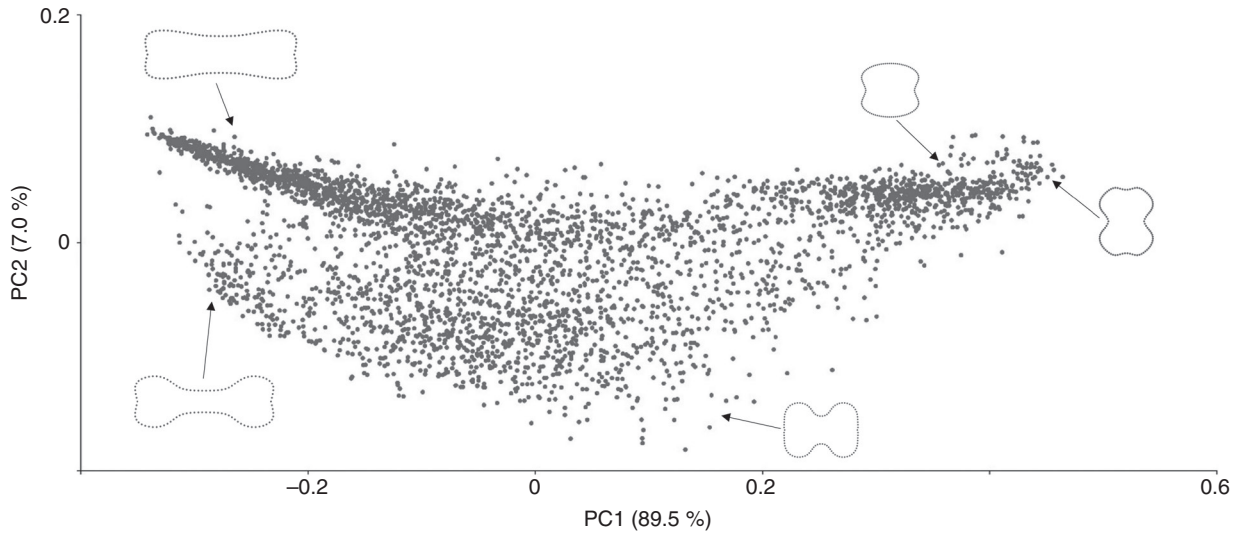

FIG. 3. Principal component analysis of 3650 symmetric phytolith shape configurations. Dots indicate individual phytoliths. The first two PCs are associated with the most pronounced shape variation within the dataset. This shape variation is visualized by phytolith outlines.

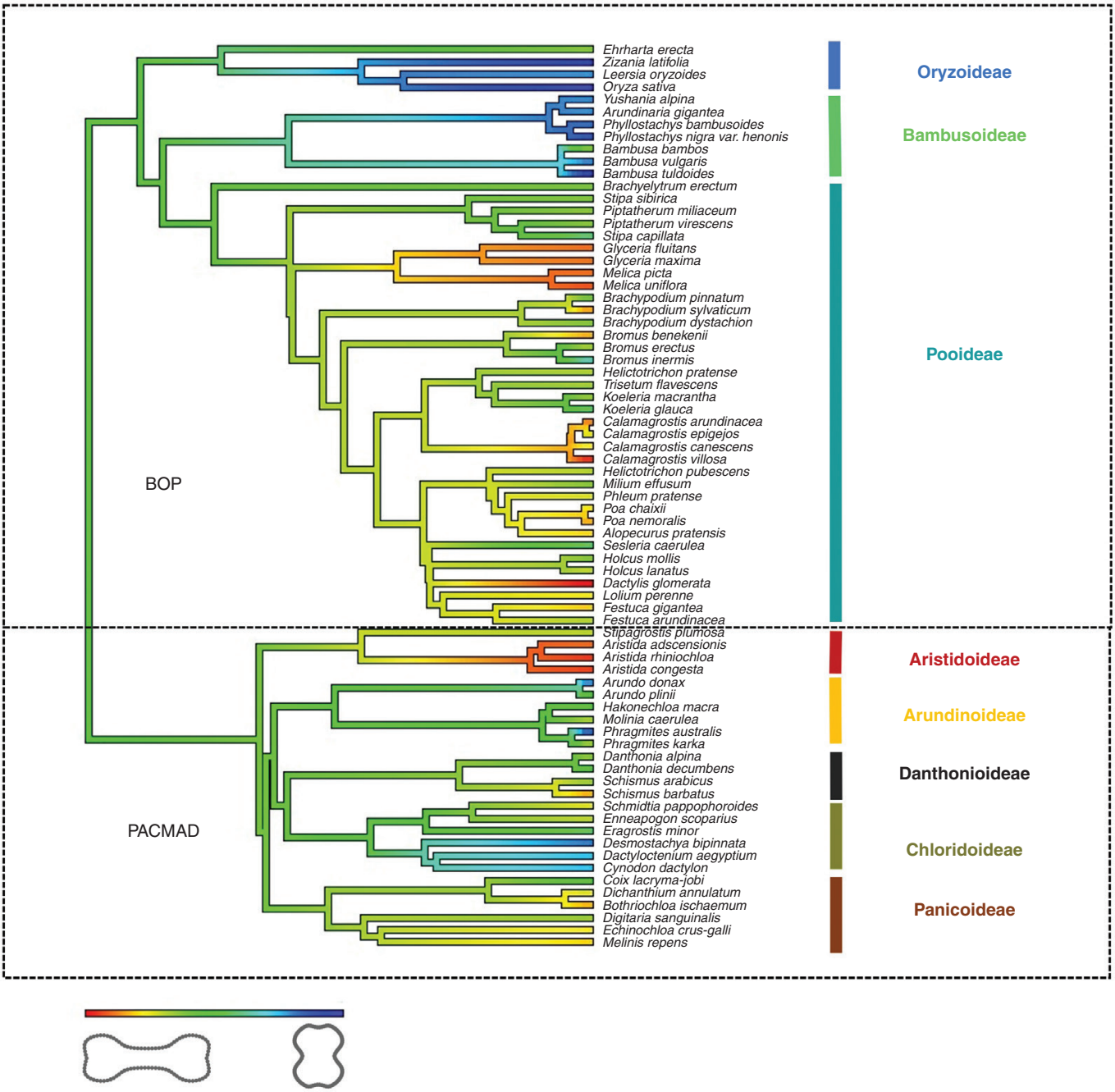

FIG. 4. Phytolith shape variation pattern across grass phylogeny. Grass phylogeny was constructed with the V.PhyloMaker package in R (Jin and Qian, 2019); 'backbone' tree based on molecular data from seed plant phylogeny (mega-tree 'GBOTB.extended.tre'; Smith and Brown, 2018). Grass species positions along the first principal component axis (PC1) were mapped on the tree. The colour scale indicates grass silica short cell phytolith shape variation along PC1.

DISCUSSION

The observed evolutionary pattern in phytolith shape

In general, the results of this study concur with previous reports that GSSC phytolith shapes closely reflect phylogenetic relationships between taxa (Piperno and Pearsall, 1998; Gallaher *et al.*, 2020). Poaceae phytolith shape changed along with other anatomical and micromorphological leaf traits in response to their diversification in the course of evolutionary history (Thomasson, 1978; Romaschenko, 2011; Rudall *et al.*, 2014). The deep-time diversification of grass subfamilies is the main driver of phytolith shape variation. Modern grasses produce phytoliths similar in shape to those produced by their ancestors (Thomasson, 1987; Strömberg, 2005; Prasad *et al.*, 2005, 2011).

We found differences between subfamilies known for their distinct phytolith shape (Chloridoideae, Oryzoideae, Bambusoideae, Panicoideae and Pooideae; Twiss *et al.*,

TABLE 2. *Measure of phylogenetic conservatism in phytolith shape. Symmetric variation (PC1–PC4), asymmetric variation (vertical, left-right and transversal) and intraindividual variation in symmetrized phytolith shapes were evaluated*

Type of shape variation	Proportion of variation (PCA)	(%)	Pagel's lambda (λ)	Lower 95 % CI	Upper 95 % CI
Symmetric	PC1	89.5	0.686	0.453	0.843
	PC2	7.0	0.517	0.208	0.753
	PC3	1.5	0.523	0.236	0.75
	PC4	1.0	0.486	0.083	0.764
Intraindividual symmetric	–	–	0.428	0.053	0.744
Asymmetric	Vertical	1.9	0.188	NA	0.627
	Left–right	2.4	6×10^{-5}	NA	0.219
	Transversal	6.7	6×10^{-5}	NA	0.455

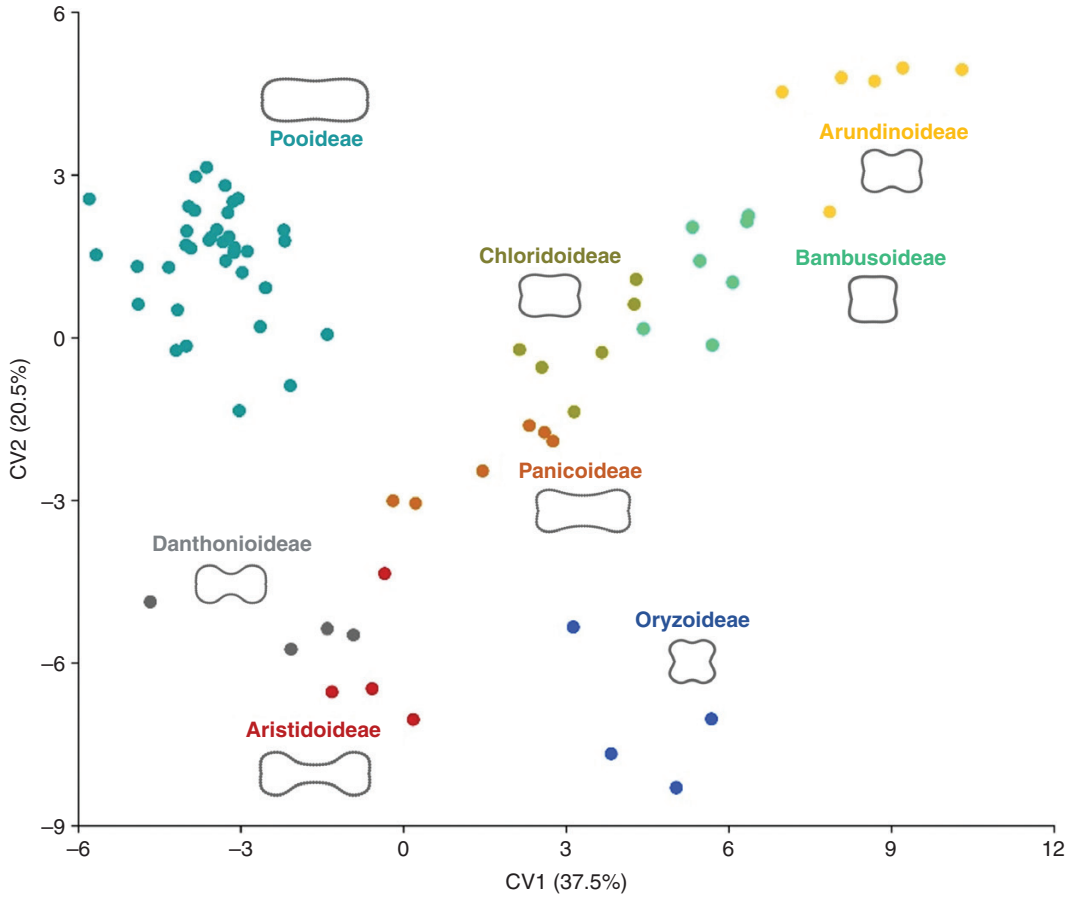

FIG. 5. Canonical variates analysis used to discriminate between symmetrized phytolith shapes of grass subfamilies. The phylogenetic signal in the shape data is apparent from the distinctive position of individual grass subfamilies in the morphospace. Dots represent centroids for species.

1969; Gallaher *et al.*, 2020), but also between smaller subfamilies such as Aristidoideae, Arundinoideae and Danthonioideae. We also revealed phytolith shape diversification in some tribes. Axially oriented bilobate-shaped phytoliths of *Ehrharta erecta* (Ehrharteae) differed from those in Oryzoideae, while *Oryza sativa*, *Zizania latifolia* and *Leersia oryzoides* (Oryzeae) formed a separate cluster within this subfamily. Similarly, bilobate-shaped phytoliths of *Eragrostis minor* and *Enneapogon scoparius* (Eragrostideae) differed from those in Chloridoideae. Also, *Stipa* and *Piptatherum* (Stipeae) and *Melica* and *Glyceria* (Meliceae) differed from Pooideae. Further analysis of phytolith shape examining a wider range of grass tribes would be useful.

This study had the advantage of using phytoliths still bound within leaf material, so the orientation of each phytolith in the leaf was known. However, the majority of phytolith studies work with phytoliths isolated from leaves. Orientation of phytoliths within the epidermis is crucial in phytolith identification (Rudall *et al.*, 2014). For example, subfamily Oryzoideae

is characterized by tall, transversally oriented, bilobate-shaped phytoliths (with scooped ends in tribe Oryzeae) (Prasad *et al*., 2005, 2011). However, in this study, 2-D phytolith outlines of Oryzoideae would be nearly indistinguishable from bilobate-shaped phytolith outlines in other subfamilies if the orientation within the leaf was not known. To preserve taxonomic information in 2-D phytolith outlines obtained from isolated phytoliths, we need to infer the original orientation of Oryzoideae phytoliths from their 3-D characteristics (Neumann *et al.*, 2017; Gallaher *et al.*, 2020).

Intraindividual variation in relation to the phylogenetic pattern in phytolith shape

While the phylogenetic signal in intraindividual variation in phytolith shape was generally low, we still detected a remarkable pattern in the distribution of intraindividual variation across grass phylogeny. The phytolith shapes of *E. minor* were the most variable, producing both saddle-shaped phytoliths characteristic of its subfamily Chloridoideae and bilobate-shaped phytoliths generally attributed to Panicoideae. Researchers have attributed high intraindividual variation in *Eragrostis* species to their position in the phylogenetic tree diverging early from Chloridoideae (Piperno and Pearsall, 1998). Similarly, highly variable polylobate-shaped phytoliths occurred in *Ehrharta*, which diverged early from Oryzoideae. In Pooideae, the early-diverging lineages (Brachyelytrum, Brachypodieae, Bromeae and Meliceae) also varied significantly in phytolith shape. However, we also found highly variable phytolith shapes in core groups (e.g. Poeae, Andropogoneae) and very conservative phytolith shapes in early-diverging lineages (e.g. Aristideae). Further studies of phylogenetic signals in intraindividual phytolith shape variation are needed to clarify these patterns.

Regardless of a phylogenetic signal in intraindividual phytolith shape variation, possible variation must be considered when classifying fossil phytoliths. Should fossil taxa be classified by comparing them with average phytolith shape (representing whole intraindividual shape variation for a single shape) or by comparing them with the whole intraindividual phytolith shape variation within the species of our reference collection? Our study suggests that the second option is better since the average phytolith shape of some species does not necessarily reflect the natural variation in phytolith shape (as seen in the extreme case of *E. minor*). A reference collection based on the entire range of intraindividual phytolith shape variation of the studied species is required.

The ecological component in phytolith shape variation

Although we found a clear phylogenetic signal in phytolith shape, we were surprised by large differences in phytolith shapes (particularly between elongated and shorter shapes) found in certain closely related taxa. Grass long cell phytoliths, similar to crenate and polylobate GSSC phytoliths in some species, are consistently larger and proportionally longer in reduced light conditions (Dunn *et al.*, 2015). Researchers have suggested that the addition of trichomes and stomata to the epidermis might shorten phytoliths, and that the densities of both stomata and trichomes increase with enhanced light conditions in grasses (Allard *et al.*, 1991; Knapp and Gilliam, 1985). We found possible evidence for this hypothesis in the Stipeae vs. Meliceae tribes within the Pooideae subfamily. The Stipeae includes species that generally occupy drier open grasslands and steppe communities (e.g. Romaschenko *et al*., 2011, 2012). Meliceae is mostly found in shady woodlands or wet environments. More studies focusing on phytolith shape variation along environmental gradients and comparison with other anatomical traits (e.g. stomata and trichome densities) is required to further test this hypothesis; however, our study suggests that this shape variation results more from long-term ecological adaptation of species within these tribes than a short-term plastic response of phytolith shape to the environment.

Limitations of current study

Geometric morphometrics enable quantitative assessment of phytolith shape variation and the exploration of trends in phytolith shape variation within one morphospace. However, the Procrustes superimposition of phytolith shapes is not universally applicable to all morphotypes. As shown in this study, for phytoliths with symmetric 2-D shapes, there may be two or more fixed points, typically derived from the orientation of phytoliths within plant tissue, delimiting individual symmetric curves. Phytoliths without these points, such as rondels or spheroids, are not suitable for morphometric analysis by the generalized Procrustes analysis. This limitation prevented us from including grass species that carry only these morphotypes, such as the genera *Nardus*, an early-diverging lineage of Pooideae, and *Festuca* (in particular, species with narrow leaves).

Landmark-based geometric morphometrics applied to a 3-D phytolith surface model to quantify GSSC phytolith shape partially overcomes this problem (Gallaher *et al.*, 2020). The 3-D shape assessment helps to establish the positional homology of all GSSC phytolith morphotypes, so they can be analysed within a common framework. However, 3-D morphometrics of phytoliths is based on confocal microscopy (Evett and Cuthrell, 2016), which is more expensive and time-consuming than analysis based on light microscopy. Because 2-D geometric morphometrics is cheaper and more accessible, robust studies are possible based on large datasets, particularly in paleoecology, where high numbers of phytoliths are typically used to reconstruct vegetation dynamics (Piperno, 2006; Strömberg, 2009).

Conclusions

We have shown the 2-D shape of GSSC phytoliths is highly relevant for the reconstruction of the evolution and paleoecology of Poaceae. Although we found that phytolith shape is mainly driven by the deep-time diversification of grass subfamilies, we also found distinct phytolith shape variation in early-diverging lineages of the subfamily Pooideae. Geometric morphometrics enables the quantitative assessment of the entire phytolith

shape and allows visualization of variation. Moreover, applying geometric morphometrics to 2-D phytolith shape is cheap and rapid, making it an excellent tool to process large numbers of phytolith outlines required for palaeoecological reconstruction.

SUPPLEMENTARY DATA

Supplementary data are available online at https://academic.oup.com/aob and consist of the following. Table S1: list of grass species used for analysis of grass silica short cell phytoliths within *in situ* charred epidermis. Table S2: workflow sequence of landmark-based geometric morphometrics and other methods used in the current study. Table S3: tests of significant difference in phytolith shape between the subfamilies. Table S4: the 'lollipop' graphs visualizing the amount of intraindividual variation in phytolith shape for all grass species under study. Table S5: linear discriminant analysis based on the first 27 PCs classified by subfamilies. Table S6: linear discriminant analysis based on the first 27 PCs classified by tribes in subfamily Pooideae. Figure S1: workflow sequence of landmark-based geometric morphometrics performed on phytoliths with biradial symmetry. Figure S2: pattern in the amount of intraindividual phytolith shape variation across grass phylogeny.

ACKNOWLEDGEMENTS

We thank Tomáš Herben at the Charles University in Prague for his help in every stage of conducting this study, including the study planning, analyses and fruitful comments on the drafts of the paper. We also thank the Herbarium Collections of the Charles University in Prague for providing the grass specimens; we thank Pavel Zdvořák, in particular, who kindly provided every grass species we needed. We would like to thank both anonymous referees for their valuable and knowledgeable comments on the final manuscript. We thank Matthew Nicholls for his diligent proofreading of the final manuscript. K.H. conceived the study, conducted imaging and data analysis. K.H. and A.P. collected plant material in the field. J.N. developed the scripts for automated analysis of phytolith shape with biradial symmetry and Procrustes ANOVA. K.H. wrote the text with the contribution of J.N., P.P. and A.P. All authors approved the final version of the manuscript.

LITERATURE CITED

Adams DC, Collyer ML, Kaliontzopoulou A, Balken E. 2021. *Geomorph: software for geometric morphometric analyses*. R package version 3.3.2.

Allard G, Nelson CJ, Pallardy SG. 1991. Shade effects on growth of tall fescue: I. Leaf anatomy and dry matter partitioning. *Crop Science* **31**: 163–167.

Alexandre A, Meunier JD, Lézine AM, Vincens A, Schwartz D. 1997. Phytoliths: indicators of grassland dynamics during the late Holocene in intertropical Africa. *Palaeogeography, Palaeoclimatology, Palaeoecology* **136**: 213–229.

Ball TB, Davis A, Evett RR, *et al.* 2016. Morphometric analysis of phytoliths: recommendations towards standardization from the International Committee for Phytolith Morphometrics. *Journal of Archaeological Science* **68**: 106–111.

Barboni D, Bremond L, Bonnefille R. 2007. Comparative study of modern phytolith assemblages from inter-tropical Africa. *Palaeogeography, Palaeoclimatology, Palaeoecology* **246**: 454–470.

Bookstein FL. 1989. Principal warps: thin-plate splines and the decomposition of deformations. *IEEE Transactions in Pattern Analysis and Machine Intelligence* **11**: 567–585.

Bookstein FL. 1997. Landmark methods for forms without landmarks: morphometrics of group differences in outline shape. *Medical Image Analysis* **1**: 225–243.

Bouchenak-Khelladi Y, Verboom GA, Savolainen V, Hodkinson TR. 2010. Biogeography of the grasses (Poaceae): a phylogenetic approach to reveal evolutionary history in geographical space and geological time. *Botanical Journal of the Linnean Society* **162**: 543–557.

Bremond L, Alexandre A, Hély C, Guiot J. 2005. A phytolith index as a proxy of tree cover density in tropical areas: calibration with Leaf Area Index along a forest–savanna transect in southeastern Cameroon. *Global and Planetary Change* **45**: 277–293.

Cai Z, Ge S. 2017. Machine learning algorithms improve the power of phytolith analysis: a case study of the tribe Oryzeae (Poaceae). *Journal of Systematics and Evolution* **55**: 377–384.

Diester-Haass L, Schrader HJ, Thiede J. 1973. Sedimentological and paleoclimatological investigations of two pelagic ooze cores off Cape Barbas, North-West Africa. *Meteor Forshungergebnisse* **16**: 19–66.

Dryden IL. Mardia KV. 2016. *Statistical shape analysis, with applications in R*, 2nd edn. Chichester, UK: Wiley.

Dunn RE, Le TY, Strömberg CA. 2015. Light environment and epidermal cell morphology in grasses. *International Journal of Plant Sciences* **176**: 832–847.

Edwards EJ, Smith SA. 2010. Phylogenetic analyses reveal the shady history of C4 grasses. *Proceedings of the National Academy of Sciences, USA* **107**: 2532–2537.

Evett RR, Cuthrell RQ. 2016. A conceptual framework for a computer-assisted, morphometric-based phytolith analysis and classification system. *Journal of Archaeological Science* **68**: 70–78.

Fahmy AG. 2008. Diversity of lobate phytoliths in grass leaves from the Sahel region, West Tropical Africa: Tribe Paniceae. *Plant Systematics and Evolution* **270**: 1–23.

Fredlund GG, Tieszen LT. 1994. Modern phytolith assemblages from the North American great plains. *Journal of Biogeography* **21**: 321–335.

Gallego L, Distel RA. 2004. Phytolith assemblages in grasses native to central Argentina. *Annals of Botany* **94**: 865–874.

Gallaher TJ, Akbar SZ, Klahs PC, *et al.* 2020. 3D shape analysis of grass silica short cell phytoliths: a new method for fossil classification and analysis of shape evolution. *New Phytologist* **228**: 376–392.

Gibson DJ. 2009. *Grasses and grassland ecology*. Oxford: Oxford University Press.

Gunz P, Mitteroecker P. 2013. Semilandmarks: a method for quantifying curves and surfaces. *Hystrix, the Italian Journal of Mammalogy* **24**: 103–109.

Hammer Ø, Harper DAT, Ryan PD. 2001. PAST: paleontological statistics software package for education and data analysis. *Palaeontologia Electronica* **4**: 9.

Hošková K, Pokorná A, Neustupa J, Pokorný P. 2021. Inter- and intraspecific variation in grass phytolith shape and size: a geometric morphometrics perspective. *Annals of Botany* **127**: 191–201.

International Committee for Phytolith Taxonomy (ICPT). 2019. International code for phytolith nomenclature (ICPN) 2.0. *Annals of Botany* **124**: 189–199.

Jacobs BF, Kingston JD, Jacobs LL. 1999. The origin of grass-dominated ecosystems. *Annals of the Missouri Botanical Garden* **86**: 590–643.

Jin Y, Qian H. 2019. V. PhyloMaker: an R package that can generate very large phylogenies for vascular plants. *Ecography* **42**: 1353–1359.

Klingenberg CP. 2011. MorphoJ: an integrated software package for geometric morphometrics. *Molecular Ecology Resources* **11**: 353–357.

Klingenberg CP. 2013. Visualization in geometric morphometrics: how to read and how to make graphs showing shape changes. *Hystrix, the Italian Journal of Mammalogy* **24**: 15–24.

Klingenberg CP. 2015. Analyzing fluctuating asymmetry with geometric morphometrics: concepts, methods, and applications. *Symmetry* **7**: 843–934.

Knapp AK, Gilliam FS. 1985. Response of *Andropogon gerardii* (Poaceae) to fire-induced high vs. low irradiance environments in tallgrass prairie: leaf structure and photosynthetic pigments. *American Journal of Botany* **72**:1668–1671.

Kumar S, Milstein Y, Brami Y, Elbaum M, Elbaum R. 2017. Mechanism of silica deposition in sorghum silica cells. *New Phytologist* **213**: 791–798.

Lu H, Liu KB. 2003. Morphological variations of lobate phytoliths from grasses in China and the south-eastern United States. *Diversity and Distributions* **9**: 73–87.

Mander L, Li M, Mio W, Fowlkes CC, Punyasena SW. 2013. Classification of grass pollen through the quantitative analysis of surface ornamentation and texture. *Proceedings of the Royal Society B: Biological Sciences* **280**: 1–7.

Metcalfe CR. 1960. *Anatomy of the monocotyledons. I. Gramineae*. Oxford: Clarendon Press.

Mitteroecker P, Bookstein F. 2011. Linear discrimination, ordination, and the visualization of selection gradients in modern morphometrics. *Evolutionary Biology* **38**: 100–114.

Mulholland SC. 1989. Phytolith shape frequencies in North Dakota grasses: a comparison to general patterns. *Journal of Archaeological Science* **16**: 489–511.

Mulholland SC, Rapp G Jr. 1992. A morphological classification of grass silica bodies. In: Rapp G Jr, Mulholland SC, eds. *Phytolith systematics: emerging issues. Advances in archaeological and museum science*, **Vol. 1**. Boston, MA: Springer, 65–89.

Neumann K, Fahmy AG, Müller-Scheeßel N, Schmidt M. 2017. Taxonomic, ecological and palaeoecological significance of leaf phytoliths in West African grasses. *Quaternary International* **434**: 15–32.

Neustupa J. 2013. Patterns of symmetric and asymmetric morphological variation in unicellular green microalgae of the genus *Micrasterias* (Desmidiales, Viridiplantae). *Fottea* **13**: 53–63.

Neustupa J, Woodard K. 2021. Male sterility significantly elevates shape variation and fluctuating asymmetry of zygomorphic corolla in gynodioecious *Glechoma hederacea* (Lamiaceae). *AoB Plants* **13**: plab013.

Novello A, Barboni D, Berti-Equille L, Mazur JC, Poilecot P, Vignaud P. 2012. Phytolith signal of aquatic plants and soils in Chad, Central Africa. *Review of Palaeobotany and Palynology* **178**: 43–58.

Oksanen J, Blanchet FG, Friendly M, *et al.* 2019. vegan: *community ecology package*. R package version 2.5-6.

Orme D, Freckleton R, Thomas G, *et al.* 2018. *caper: comparative analyses of phylogenetics and evolution in R*. R package version 1.0.1.

Pérez R, De Ciurana J, Riba C. 2006. The characterization and specification of functional requirements and geometric tolerances in design. *Journal of Engineering Design* **17**: 311–324.

Piperno DR. 2006. *Phytoliths: a comprehensive guide for archaeologists and paleoecologists*. Lanham, MD: Altamira Press.

Piperno DR, Pearsall DM. 1998. The silica bodies of tropical American grasses: morphology, taxonomy, and implications for grass systematics and fossil phytolith identification. *Smithsonian Contributions to Botany* **85**: 1–40.

Polly PD, Motz GJ. 2016. Patterns and processes in morphospace: geometric morphometrics of three-dimensional objects. *The Paleontological Society Papers* **22**: 71–99.

Prasad V, Strömberg CA, Alimohammadian H, Sahni A. 2005. Dinosaur coprolites and the early evolution of grasses and grazers. *Science* **310**: 1177–1180.

Prasad V, Strömberg CAE, Leaché AD, *et al.* 2011. Late Cretaceous origin of the rice tribe provides evidence for early diversification in Poaceae. *Nature Communications* **2**: 1–9.

R Core Team. 2020. *R: a language and environment for statistical computing*. Vienna, Austria: R Foundation for Statistical Computing.

Revell LJ. 2012. phytools: an R package for phylogenetic comparative biology (and other things). *Methods in Ecology and Evolution* **3**: 217–223.

Rohlf FJ. 2015. The tps series of software. *Hystrix, the Italian Journal of Mammalogy* **26**: 9–12.

Romaschenko K, Peterson PM, Soreng RJ, Futorna O, Susanna A. 2011. Phylogenetics of *Piptatherum* s. l. (Poaceae: Stipeae): evidence for a new genus, *Piptatheropsis*, and resurrection of *Patis*. *Taxon* **60**: 703–1716.

Romaschenko K, Peterson PM, Soreng RJ, Garcia-Jacas N, Futorna O, Susanna A. 2012. Systematics and evolution of the needle grasses (Poaceae: Pooideae: Stipeae) based on analysis of multiple chloroplast loci, ITS, and lemma micromorphology. *Taxon* **61**: 18–44.

Rovner I, Russ JC. 1992. Darwin and design in phytolith systematics: morphometric methods for mitigating redundancy. In: Mulholland SC, Rapp G, eds. *Phytolith systematics: emerging issues. Advances in archaeological and museum science*, **Vol. 1**. Boston, MA: Springer, 253–276

Rudall PJ, Prychid CJ, Gregory T. 2014. Epidermal patterning and silica phytoliths in grasses: an evolutionary history. *Botanical Review* **80**: 59–71.

Russ JC, Rovner I. 1989. Stereological identification of opal phytolith populations from wild and cultivated *Zea*. *American Antiquity* **54**: 784–792.

Savriama Y. 2018. A step-by-step guide for geometric morphometrics of floral symmetry. *Frontiers in Plant Science* **9**: 1433.

Savriama Y, Klingenberg CP. 2011. Beyond bilateral symmetry: geometric morphometric methods for any type of symmetry. *BMC Evolutionary Biology* **11**: 280.

Savriama Y, Gómez JM, Perfectti F, Klingenberg CP. 2012. Geometric morphometrics of corolla shape: dissecting components of symmetric and asymmetric variation in *Erysimum mediohispanicum* (Brassicaceae). *New Phytologist* **196**: 945–954.

Savriama Y, Neustupa J, Klingenberg CP. 2010. Geometric morphometrics of symmetry and allometry in *Micrasterias rotata* (Zygnemophyceae, Viridiplantae). *Nova Hedwigia* **136**: 43–54.

Schaefer K, Lauc T, Mitteroecker P, Gunz P, Bookstein FL. 2006. Dental arch asymmetry in an isolated Adriatic community. *American Journal of Physical Anthropology* **129**: 132–142.

Schubert M, Grønvold L, Sandve SR, Hvidsten TR, Fjellheim S. 2019*a*. Evolution of cold acclimation and its role in niche transition in the temperate grass subfamily Pooideae. *Plant Physiology* **180**: 404–419.

Schubert M, Marcussen T, Meseguer AS, Fjellheim S. 2019*b*. The grass subfamily Pooideae: Cretaceous–Palaeocene origin and climate-driven Cenozoic diversification. *Global Ecology and Biogeography* **28**: 1168–1182.

Silantyeva M, Solomonova M, Speranskaja N, Blinnikov MS. 2018. Phytoliths of temperate forest–steppe: a case study from the Altay, Russia. *Review of Palaeobotany and Palynology* **250**: 1–15.

Smith SA, Brown JW. 2018. Constructing a broadly inclusive seed plant phylogeny. *American Journal of Botany* **105**: 302–314.

Soreng RJ, Peterson PM, Romaschenko K, *et al.* 2015. A worldwide phylogenetic classification of the Poaceae (Gramineae). *Journal of Systematics and Evolution* **53**: 117–137.

Soreng RJ, Peterson PM, Romaschenko K, *et al.* 2017. A worldwide phylogenetic classification of the Poaceae (Gramineae) II: an update and a comparison of two 2015 classifications. *Journal of Systematics and Evolution* **55**: 259–290.

Strömberg CAE. 2005. Decoupled taxonomic radiation and ecological expansion of open-habitat grasses in the Cenozoic of North America. *Proceedings of the National Academy of Sciences, USA* **102**: 11980–11984.

Strömberg CAE. 2009. Methodological concerns for analysis of phytolith assemblages: does count size matter? *Quaternary International* **193**: 124–140.

Strömberg CAE. 2011. Evolution of grasses and grassland ecosystems. *Annual Review of Earth and Planetary Sciences* **39**: 517–544.

Strömberg CAE, Dunn RE, Crifò C, Harris EB. 2018. Phytoliths in paleoecology: analytical considerations, current use, and future directions. In: Croft DA, Su DF, Simpson SW, eds. *Methods in paleoecology: reconstructing cenozoic terrestrial environments and ecological communities*. Cham, Switzerland: Springer, 235–287.

Thomasson JR. 1978. Epidermal patterns of the lemma in some fossil and living grasses and their phylogenetic significance. *Science* **199**: 975–977.

Thomasson JR. 1987. Late Miocene plants from northeastern Nebraska. *Journal of Paleontology* **61**: 1065–1079.

Twiss PC. 1992. Predicted world distribution of C3 and C4 grass phytoliths. In: Rapp G Jr, Mulholland SC, eds. *Phytolith systematics: emerging issues. Advances in archaeological and museum science*, **Vol. 1**. Boston, MA: Springer, 113–128.

Twiss PC, Suess E, Smith RM. 1969. Morphological classification of grass phytoliths. *Soil Science Society of America Proceedings* **33**: 109–115.

Yost CL, Ivory SJ, Deino AL, Rabideaux NM, Kingston JD, Cohen AS. 2021. Phytoliths, pollen, and microcharcoal from the Baringo Basin, Kenya reveal savanna dynamics during the Plio-Pleistocene transition. *Palaeogeography, Palaeoclimatology, Palaeoecology* **570**: 109779.

Zelditch ML, Swiderski DL, Sheets DH. 2012. *Geometric morphometrics for biologists: a primer*, 2nd edn. London: Academic Press.